Microfluid Nanofluid (2008) 5:77–87
DOI 10.1007/s10404-007-0228-6

RESEARCH PAPER

Full field measurement at the micro-scale using micro-interferometry

Julie Garvey · David Newport · Fereydoun Lakestani · Maurice Whelan · Shiju Joseph

Received: 14 August 2007 / Accepted: 24 September 2007 / Published online: 12 October 2007

Abstract This paper presents micro-interferometry as a measurement technique to extract temperature profiles and/or mass transfer gradients rapidly and locally in micro-devices. Interferometry quantifies the phase change between two or more coherent light beams induced by temperature and/or mass concentration. Previous work has shown that temporal noise is a limiting factor in microscale applications. This paper examines phase stepping and heterodyne phase retrieval techniques with both CCD and CMOS cameras. CMOS cameras are examined owing to the high speed at which images can be acquired which is particularly relevant to heterodyne methods. It is found that heterodyne retrieval is five times better than phase stepping being limited to 0.01 rad or $\lambda/628$. This is twice the theoretical limit of $\lambda/1{,}000$. The technique is demonstrated for mixing in a T-junction with a 500 μm square channel and compared favourably to a theoretical prediction from the literature. Further issues regarding application to temperature measurements are discussed.

Keywords Phase stepping · Heterodyne technique · Phase · Micro-channel · CMOS camera · Micro-mixing

J. Garvey · D. Newport (✉) · S. Joseph
Stokes Research Institute, University of Limerick, Limerick, Ireland
e-mail: david.newport@ul.ie

S. Joseph
e-mail: shiju.joseph@ul.ie

F. Lakestani · M. Whelan
European Commission DG, Joint Research Centre, Institute for Health and Consumer Protection, 21020 Ispra, VA, Italy
e-mail: fereydoun.lakestani@ul.ie

M. Whelan
e-mail: maurice.whelan@jrc.it

Present Address:
J. Garvey
Medtronic, Parkmore Business Park West, Galway, Ireland
e-mail: julie.garvey@gmail.com

1 Introduction

There is a well-articulated need for local measurement at the microscale (Garimella and Sobhan 2002; Sato et al. 2003). This paper presents micro-interferometry as a measurement technique to extract temperature profiles and/or mass transfer gradients rapidly and locally in micro-devices.

Micro-PIV and fluorescent techniques have been developed to quantify velocity and mass transfer in liquid systems. These have not been applied to gaseous systems because of an absence of suitable fluorescent markers, (Wereley et al. 2002). There are numerous techniques currently being developed for temperature measurement at the microscale. IR thermography, (Hestroni et al. 2003; Patil and Narayanan 2005; Hapke et al. 2002), thermoreflectance (Christofferson et al. 2001), Brownian motion of micro-PIV particles (Hohreiter et al. 2002), and the use of thermochromic crystals (Chaudhari et al. 1998; Fung et al. 2006). To date, these techniques have not offered the potential for full field local measurement being restricted to surface measurements, volume emission effects, limited accuracy and for thermochromic crystals, the need for in situ calibration.

This paper builds on the earlier work of the authors (Newport et al. 2004; Garvey et al. 2004) and presents micro-interferometry as a powerful and accurate technique to quantify mixing processes in micro-devices. The issues to be resolved in obtaining temperature measurements are also

discussed. The challenges facing micro-interferometry are twofold: signal to noise, and optical access. The latter is addressed through transparent fluids and devices but restricted if large differences in the refractive index of the fluids or device exist, either resulting in a lensing or diffractive effect. The former was initially examined by Newport et al. (2004) who produced a design envelope for an interferometer. This showed that a typical phase stepping interferometer is sufficiently sensitive for temperature measurement in liquid mini-systems but inadequate for gaseous systems.

This paper presents further improvements in interferometer noise through heterodyne techniques and demonstrates the implementation to mixing in a 500 μm square channel. The paper is structured as follows: first background theory to interferometric measurement and heterodyne phase evaluation is presented, followed by details of the interferometer setup and test piece. The results are discussed in terms of noise and measurement and the paper concludes with a look at additional factors that need to be addressed to fully realise micro-interferometry for temperature and concentration measurement.

2 Theory

Generally, the interferometers employed for flow measurement employ two-beam amplitude-division interferometry (Merzkirch 1987; Mayinger 1993). The interference pattern resulting from recombining the two beams can then be expressed mathematically as,

$$I = I_1 + I_1 + 2\sqrt{I_1 I_2}\cos\delta \tag{1}$$

where, I_1 and I_2 are the beam intensities, and δ is the phase difference between the two.

Phase differences occur due to a change in optical path length caused by the measurand (temperature, pressure, strain, concentration). The objective in interferometric measurements is to determine the value of the phase difference and relate it to the measurand. Phase retrieval can be achieved through phase stepping or heterodyne techniques, described in the next subsections. It should be noted that most fluids' measurements present manual phase evaluation where the phase is evaluated at the fringe maxima and minima; this is surprising as automatic phase retrieval algorithms have been available and widely implemented in the optics community for some two decades.

The phase change in a 2D system is related to the change in refractive index through

$$\delta = \frac{2\pi L}{\lambda_0}\Delta n \tag{2}$$

where, L is the length over which the phase change takes place, for example, the depth of a micro-channel. The appropriate relationship can then be employed to relate the change in refractive index to the measurand e.g. the Gladstone–Dale equation which relates temperature to refractive index for gases or the Lorenz–Lorentz equation for liquids).

Following the traditional methods of optical metrology, one would require to analyse the fringe lines of the interferogram, to obtain the phase. This necessitates accurate quantitative interpretation of the fringe patterns. Malacara et al. (1998) have divided the different ways of obtaining phase directly, broadly in two groups, namely, phase stepping technique and heterodyne technique.

2.1 Phase stepping phase retrieval

Phase stepping involves introducing known phase steps into one of the beams of the interferometer. Typically this is achieved by physically displacing a mirror a known amount. In heterodyne techniques, as shown by Malacara et al. (1969) a frequency shift of the reference beam is used.

The phase term is not directly obtained at the detector, but has to be retrieved from the interferogram, by using phase-retrieval methods. Malacara et al. (1998) has exhaustively discussed phase-retrieval methods and algorithms of which the three-step method, the four-step method, the five-step method and the Carre method are widely used. Creath (1991) reported the five-step method to be least error-sensitive. The five-step method is used in this paper. A known phase-shift (α) is introduced in five finite discrete steps, by a suitable method. In the present study, a piezoelectric transducer attached to a plane mirror was used. If I_i is the intensity obtained at ith step, then for five steps introduced five intensity equations are obtained, as shown below

$$I_i = I_0[1 + \gamma\cos(\phi + \alpha_i)] \tag{3}$$

where, γ is the data modulation factor and recommended to be $0.05 \le \gamma \le 0.1$ Creath (1994).

Thus, if $\alpha = -\pi, -\pi/2, 0, \pi/2, \pi$, then phase

$$\phi = \arctan\left[\frac{2(I_2 - I_4)}{(2I_3 - I_5 - I_1)}\right] \tag{4}$$

However, when comparing two pixels and measuring the phase difference between them, this becomes,

$$\phi_2 - \phi_1 = \arctan\left[\frac{\tan\phi_2 - \tan\phi_1}{1 + (\tan\phi_1)(\tan\phi_2)}\right] \tag{5}$$

2.2 Heterodyne phase retrieval

The heterodyning process involves the interference of two signals. Within heterodyne interferometry, both signals

originate from the same source and both are then shifted by a frequency, f. The two signals acquired by a point detector are mathematically expressed as

$$E_1(t) = E_{01}\sin[2\pi(v_0+f_1)t]$$
$$E_2(t) = E_{02}\sin[2\pi(v_0+f_2)t] \quad (6)$$

After superposing, the interference signal effectively becomes (Massie et al. 1979);

$$I(t) = E_{01}^2\sin^2[2\pi(v_0+f_1)t] + E_{02}^2\sin[2\pi(v_0+f_2)t] + 2E_{01}E_{02}\sin[2\pi(v_0+f_1)t]\sin[2\pi(v_0+f_2)t] \quad (7)$$

Neglecting high-frequency signals ($\sim$MHz), i.e., (v_0+f_1), (v_0+f_2) and $(2v_0+f_1+f_2)$, since they are above the limit of the detector and after time-averaging, the detected signal then becomes

$$S = \frac{1}{2}E_{01}^2 + \frac{1}{2}E_{02}^2 + E_{01}E_{02}\cos[2\pi(f_1-f_2)t] \quad (8)$$

where $\frac{1}{2}E_{01}^2 + \frac{1}{2}E_{02}^2$ represents the direct current (DC) voltages acquired by the detectors and the remainder is the modulating signal at the frequency difference $f_1 - f_2$.

The phase is evaluated by analysing the difference between two pixel signals over a duration of ten periods. The integration over ten periods reduces the effect of random noises on the phase measurement.

The two pixel intensity signals are sinusoids and mathematically expressed as;

$$S_1 = A_1 + B_1\cos(2\pi\Delta ft + \phi_1 + \alpha(t))$$
$$S_2 = A_2 + B_2\cos(2\pi\Delta ft + \phi_2 + \alpha(t)) \quad (9)$$

where Δf is the carrier frequency, ϕ is the phase of the interference wave and $\alpha(t)$ is an additional phase modulation term due to translational vibrations or drifts in the system.

If $\omega = 2\pi\Delta f$; expressing the signals (Eq. 9) in Euler notation and subsequent multiplication with $e^{j\omega' t}$, gives,

$$S_1' = A_1 e^{j\omega' t} + \frac{B_1}{2}e^{+j((\omega+\omega')t+\phi_1+\alpha(t))} + \frac{B_1}{2}e^{-j((\omega-\omega')t+\phi_1+\alpha(t))}$$
$$S_2' = A_2 e^{j\omega' t} + \frac{B_2}{2}e^{+j((\omega+\omega')t+\phi_2+\alpha(t))} + \frac{B_2}{2}e^{-j((\omega-\omega')t+\phi_2+\alpha(t))} \quad (10)$$

The two first terms in both the equations in Eq. 10 are continuous waves (CW) and are eliminated by an averaging over an integer number of the carrier periods. However, a Hanning gate (Malacara et al. 1969) is applied before integration. In the presence of a Hanning gate, the two CW terms are more efficiently suppressed if the integration range is not exactly equal to ten periods of the carrier or if A_1 and B_1 (and A_2 and B_2) have sum temporal fluctuations.

This results in

$$S_1' = \frac{B_1}{2}e^{-j\phi_1}$$
$$S_2' = \frac{B_2}{2}e^{-j\phi_2} \quad (11)$$

Therefore the phase difference between the two pixel signals is

$$\phi_1 - \phi_2 = \arg\left[\frac{B_2 e^{-j\phi_2}}{B_1 e^{-j\phi_1}}\right] = \arg e^{j\Delta\phi} \quad (12)$$

which, is the argument term of the complex ratio of S_2' and S_1', from Eq. 11.

3 Experimental study

3.1 Experimental set-up of Mach-Zehnder interferometer, employing heterodyne phase retrieval and CMOS/CCD camera

Figure 1 shows the schematic representation of the Mach-Zehnder interferometer, shown in Fig. 2. It consists of Nd–YAG laser source (λ = 532 nm) whose beam is reflected by a mirror, (M1), to a beam splitter (BS1). The reflected beam is known as the reference beam and the transmitted beam as the test-arm beam. At BS1 and in all subsequent beam splitters used in the present study, 50% of light is reflected and the rest transmitted. Both the beams were then individually passed through an acousto-optic modulator (AOM).

The two AOMs were supplied with a continuous wave via a voltage-controlled oscillator that inserted an optical frequency shift of approximately 80 MHz to each laser beam. However, to achieve heterodyning, the frequency of one of the beams is shifted additionally by applying additional voltage to the respective AOM, through the oscillator controlling it. This results in a frequency difference between the transmitted and reflected beams.

The reference beam is then reflected by two other mirrors, (M2, M3), through an intensity filter, to beam splitter (BS2). The intensity filter helps in reducing the beam intensity and thus reduces the nonlinear effect of the logarithmic response of the CMOS sensor of the camera. The measurement beam reflected by the mirror attached to a piezoelectric transducer (PZT), enables the introduction of a phase step to the laser beam.

The PZT mirror is controlled by a high-power amplifier, which applies phase steps equivalent to $\pi/2$. The PZT is calibrated by applying an incremental linear voltage ramp to the PZT, via an amplifier and using peak detection. The reflected beam, from the PZT mirror, then mixes with the

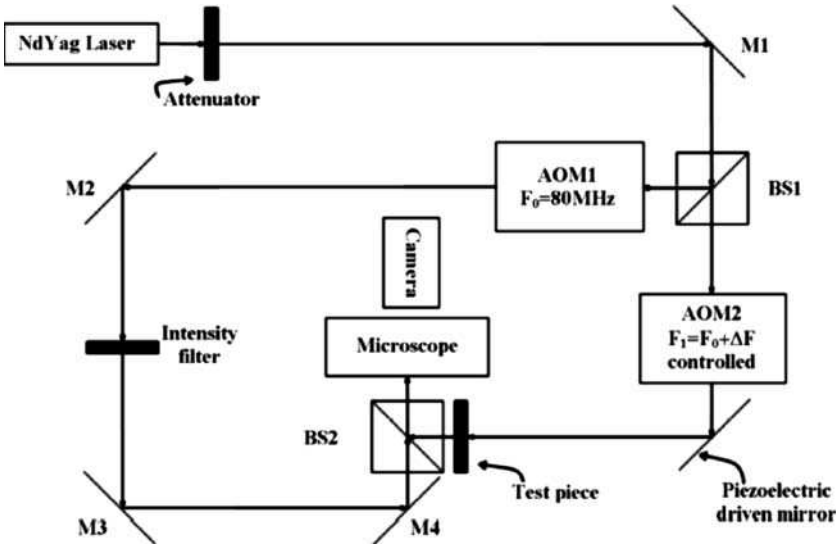

Fig. 1 Schematic of interferometric set-up for micro channel measurements

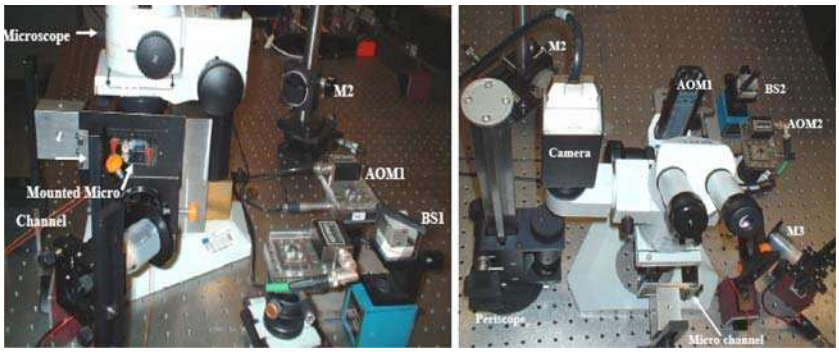

Fig. 2 Photograph of the interferometric system for micro-channel concentration measurement

reference beam through the beam splitter (BS2). The recombined beam after passing through the microscopic lens, which is focussed on the channel and thence magnifies the interference pattern in order to increase the spatial resolution of measurement, is acquired by either a CMOS or CCD camera.

3.2 Comparison and performance evaluation of heterodyne and phase stepping

For the comparative study no test piece was introduced in the system. The system was allowed to stand for 600 s and the phase-shift (in radians) during that time was measured, giving insight into the stability and uncertainty of the particular system. This experiment was repeated for heterodyne retrieval, but with additional voltage applied to one of the AOMs and no voltage applied to the PZT. A standard 1/2″ sensor CCD camera with 25 Hz sampling rate and a CMOS camera (CCAM technologies CCF15) sensor with 12.5 μm pixel pitch, providing spatial resolution of 8.9 μm at the sample level and magnification of 1.4× were used. The magnification in the CMOS camera was achieved using a microscope lens. A carrier frequency fixed at 3 Hz was used in a heterodyne interferometer with CCD camera acquisition.

When the CCD camera was used with the heterodyne interferometer, a ten-period sample of the modulating pixel signal was acquired at each measurement point, but when employed with phase stepping, an intensity measurement was taken at the pixel point, after each step. A line of 128 pixels was imaged for both the heterodyne and phase stepping interferometers.

When the CMOS camera was used with heterodyne and phase stepping, a line of 64 pixels in the CMOS camera was captured and the remaining part of the complete sensor array (512×512) was neglected thus enabling faster acquisition. When the phase stepping interferometer was operated with the CMOS camera mounted, an array of data was acquired after each phase step. However for heterodyne retrieval, a sample length of ten periods of the interference signal was acquired at each measurement point. The sampling rate of the signal was dictated by the camera and the LabVIEW interface designed for the acquisition. The LabVIEW software incorporated a code interface node, which enabled access to information written

in another language. This facilitated an interface between the CMOS camera and the LabVIEW processing program. The sampling frequency of the CMOS camera, used in heterodyne interferometer, was 500 Hz.

In order to retrieve the phase from the acquired data, the five-step technique was used (Newport et al. 2004). A discussion on phase-retrieval methods is beyond the scope of this paper and can be found in Creath (1988, 1991), Malacara et al. (1998), and Hariharan et al. (1987). Appropriate demodulation algorithms were applied to extract the phase measurements from the acquired data for both the phase-stepping and heterodyne techniques.

The data obtained by using a CCD camera for heterodyne interferometer were compared with the data obtained by using the same camera for phase stepping retrieval. The same was done with the CMOS camera. This helps in evaluating not only the technique but also the cameras.

To compare the data obtained using the CCD camera, with both the heterodyne and phase stepping techniques, the phase difference between two pixels from the array was calculated from the acquired intensity signals. The pixels chosen were pixel 0 and 50, which corresponded to a distance of 0.625 mm at the sample level. The deviation of the relative measurement over time is the phase measurement uncertainty, and this was calculated as the standard deviation of the phase measurement over time. The number of measurements varied for the two techniques as it is dependent on the measurement duration of the technique. For the phase stepping, each phase measurement consisted of the acquisition of four samples and the total measurement took 0.8 s. For heterodyne, 84 samples were acquired and the total measurement time was 3.8 s. Therefore, the phase stepping test consisted of 700 measurements and the heterodyne test comprised 160 measurements.

To compare the data obtained using the CMOS camera, the relative phase difference between two pixels was repeatedly measured over 10 min. The two pixels compared were 50 pixels apart, which is equivalent to 0.45 mm at the sample level. The number of measurements in the complete test varied for the two techniques, as it is dependent on the measurement duration of the technique. Each heterodyne measurement took 0.4 s and the phase stepping measurement took 1 s, therefore the heterodyne measurement was repeated 1,500 times and the phase stepping measurement was repeated 600 times.

3.3 500 μm square channel

Figure 3 shows a photograph of the micro-channel system. A 500 μm × 500 μm square and 80 mm long channel was machined in a transparent polycarbonate sheet with the main channel section machined as a slot through it. The resulting channel, 500 μm in depth and height, was sealed using clearseal film. The polyolefin adhesive film is 0.05 mm in thickness and provides optical access to the centre of the channel. Surface-mounted fittings were used as inlet ports to the channel block. Fluid 1, water, enters the channel at inlet 1 and fluid 2, 0.2 mol/L NaCl solution, at inlet 2. Both fluids travel from their respective inlets and coalesce at the micro-fluidic T-junction (Fig. 3) and flows adjacent to one another to the outlet. This system was placed as a test piece, in the interferometric set-up (Fig. 2).

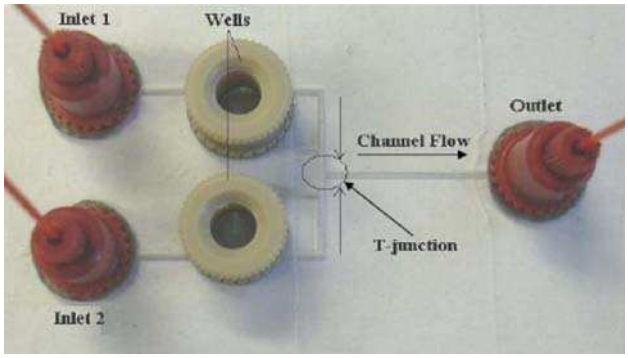

Fig. 3 Photograph of the 500 μm channel with surface mounted fittings

The flow rate of the two fluids was controlled via Becton Dickinson plastic syringes using a Harvard Apparatus PHD 22/2000 Syringe Pump. The syringes were connected to the surface mounted fittings via 1/32″ PEEK tubing with an inside diameter of 0.5 mm.

3.4 Effect of Reynolds number on the concentration profile

For this study the flow-rate of NaCl and water solution was the same and steady. The entry length for the present channel is calculated to be 380 μm and after which the flow is considered fully developed. The entry length was calculated using Dombrowski et al. (1993) equation

$$L_e = D_h(0.379\mathrm{e}^{-0.148\mathrm{Re}} + 0.0550\mathrm{Re} + 0.260) \quad (13)$$

where D_h is the hydraulic diameter and Re is the Reynolds number of the channel flow.

The phase was measured across a line of 256 pixels 4.87 mm from the inlet. To eliminate any residual phase in the system a profile should be measured initially, with the channel containing only water and then subtracted from each subsequent measurement of the binary fluid flow, to obtain the concentration profile across the channel (Garvey et al. 2004). The profile measurement was carried out for different rates (namely, 100, 50, 25, 10, 5, 2 and 1 μL/min); with both fluids having the same flow rates. The flow

rates correspond to Reynolds numbers of 6.79, 3.39, 1.70, 0.68, 0.34, 0.14 and 0.07, respectively.

For the 500 μm channel, a CMOS camera sensor with a 12.5 μm pixel pitch providing spatial resolution of 4.1 μm at the sample level and magnification of 3.05×, was used. The magnification was achieved by changing the focal length of the objective lens of the microscope. To implement heterodyne retrieval a carrier frequency, Δf, of 27 Hz was used in the system and the CMOS camera operated at a sampling frequency of 500 Hz.

4 Results and discussions

4.1 Comparison of heterodyne and phase stepping interferometry with CCD camera

Figure 4 shows the uncertainty in and comparison of phase resolution obtained in heterodyne and phase step interferometry, using the CCD camera and with no test section inserted in the system (Figs. 1, 2). The average phase values were subtracted for convenience for graphical comparison. The phase measurement reproducibility is measured over the total time of 600 s. Over the period of 600 s, the phase uncertainty of the phase stepping measurement is 0.0949 rad but for the heterodyne its 0.0167 rad. The test is repeated and the results summarised in Table 1. As from the table, the temporal deviation for the heterodyne technique is six times less than that for the phase stepping technique over a test time of 600 s. However, most real system measurement tests would not take a time of 600 s and so a calculation of the uncertainty over a shorter time of 12 s is carried out (see Table 1). Again the temporal deviation of the heterodyne technique is six times less than that for the phase stepping technique.

Table 1 Phase measurement reproducibility of phase stepping and heterodyne interferometry measurements

Test	Deviation 600 s (rad)	Deviation 12 s (rad)
Heterodyne test 1	0.0167	0.0041
Heterodyne test 2	0.0275	0.0145
Phase stepping test 1	0.0949	0.0726
Phase stepping test 2	0.1555	0.0537
Heterodyne average	0.0221	0.0093
Phase stepping average	0.1252	0.0632

The slow temporal deviations, which are present in the plots, are very probably related to temperature changes which generate beam bending and rotation and an actual phase difference between two pixels. This is not an error on the phase measurement itself but inserts an error on the index change.

The comparison of the phase measurement uncertainty in phase stepping and heterodyne techniques leads to the conclusion that higher resolution and precision could be obtained using heterodyne technique. In more traditional heterodyne systems, the carrier frequency is significantly higher than 3 Hz. However, this system and analysis demonstrated the potential of the heterodyne technique for high-resolution phase measurement.

4.2 Comparison of heterodyne and phase stepping interferometry with CMOS camera

Figure 5 shows the deviation of the phase measurement for both the heterodyne and phase stepping techniques with a CMOS detector. The complete array of results for the three tests carried out on both the heterodyne and phase stepping

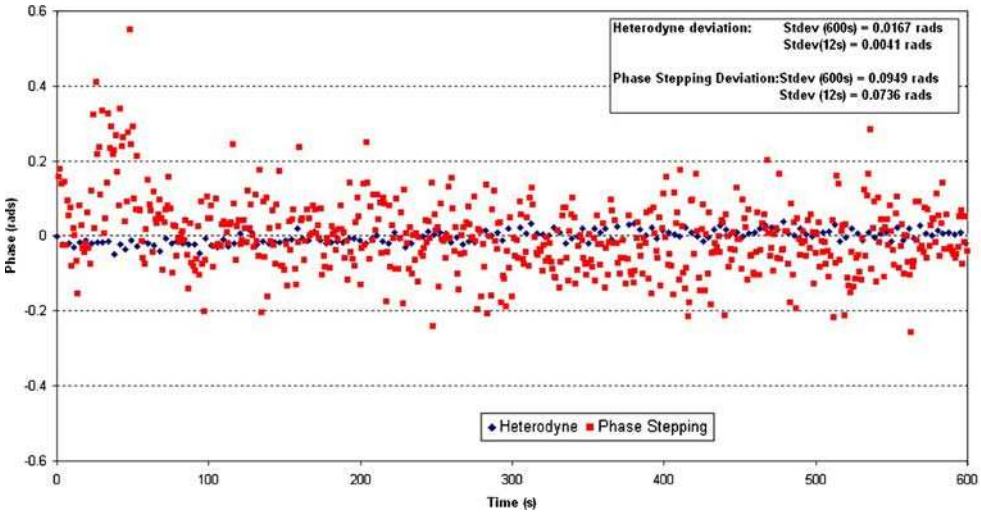

Fig. 4 Temporal variation of phase measurement resolution in heterodyne and phase stepping technique, with both using CCD detector

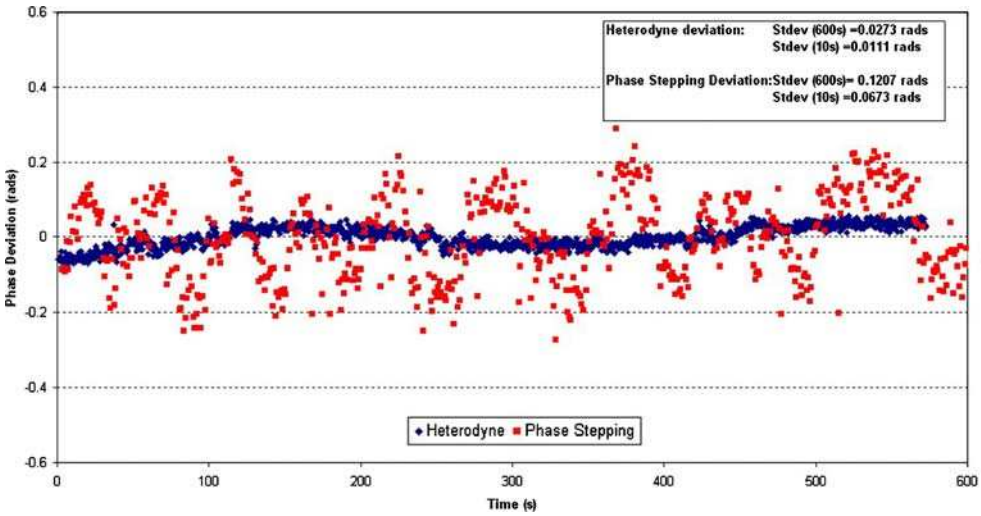

Fig. 5 Comparison of the temporal deviation of phase difference between two pixels using the heterodyne technique and the phase stepping technique

techniques are shown in Table 2. As can be seen from Fig. 5, the deviation of the phase measurement for the heterodyne technique is less than that for the phase stepping technique. From Table 2, the average phase measurement uncertainty for the heterodyne technique over a period of 600 s is 0.021 rad, while that for the phase stepping measurement was 0.1192 rad. The phase measurement uncertainty is also calculated over the shorter interval of 10 s to ascertain the effect of error on shorter measurement duration. The uncertainty of the heterodyne technique measurements had an average value of 0.0098 rad for the three tests. However, the phase stepping measurement had an average deviation of 0.0625 rad over 10 s.

The phase measurement reproducibility is a performance limitation of the system. From this analysis, the phase measurement limit of the phase stepping technique is over five times worse than it is for the heterodyne technique. For a more rapid measurement time, such as 10 s, the limit for the heterodyne technique is 0.01 rad corresponding to a resolution of $\lambda/628$. The resolution achieved by the present phase stepping technique of $\lambda/104$ is within the reported limit (Creath 1994) and the resolution achieved by the heterodyne technique is six times greater and just twice the resolution limit of $\lambda/1{,}000$ (Kafri 1989).

With higher resolving power and lower noise level, heterodyne interferometer is a useful tool for quantifying microscale phenomena. This has been verified by measuring the variation of concentration of NaCl across a micro-channel, with variation of the flow-velocity.

Table 2 Phase measurement reproducibility of heterodyne and phase stepping techniques

Test	Deviation 600 s (rad)	Deviation 10 s (rad)
Heterodyne test 1	0.0273	0.0111
Heterodyne test 2	0.018	0.0095
Heterodyne test 3	0.0176	0.0088
Phase stepping test 1	0.1207	0.0673
Phase stepping test 2	0.1198	0.0641
Phase stepping test 3	0.1172	0.0560
Heterodyne average	0.021	0.0098
Phase stepping average	0.1192	0.0625

4.3 Mapping the concentration profile of NaCl solution, across a microchannel using heterodyne Interferometry

Figure 6 shows the concentration profiles across the channel depth at 487 μm from the inlet at varied flow rates. The figure has been normalised between the concentration values of 0.2 mol/L and zero NaCl concentration for graphical convenience. Each plot is taken as a steady state measurement of the concentration profile at a constant flow rate. The graph shows that the concentration gradient decreases with the Reynolds number. This is attributed to the residency time, as it increased the amount of diffusion taking place across the channel also increases. The normalized concentration gradient measured across the channel at a Reynolds number of 6.79 is 0.13 m^{-1} however; the concentration gradient at Reynolds number of 3.39 is 0.10 m^{-1}. The concentration gradient decreases further as the Reynolds number decreases. For Re = 0.07 the normalized concentration gradient reduces to 0.002 m^{-1}. At this fluid velocity, the two fluids have almost totally mixed to a concentration of 50% NaCl solution at the point of measurement.

Figure 7 shows a comparison with theoretical predictions for the maximum and minimum profiles with a predictive equation presented by Galambos and Forster (1998). There is an offset between the predicted and

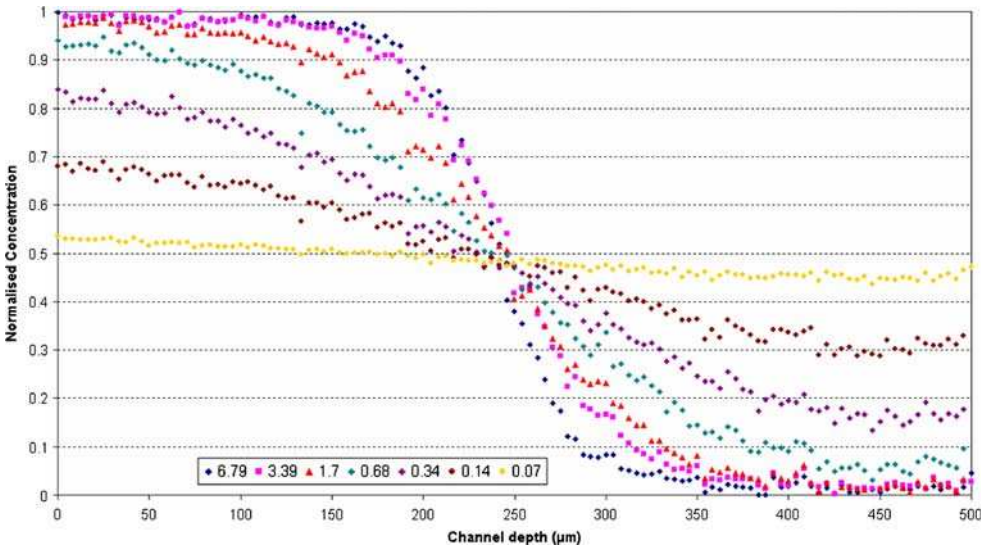

Fig. 6 Normalized concentration profile across the channel, at 487 μm from the inlet, with various Reynolds numbers

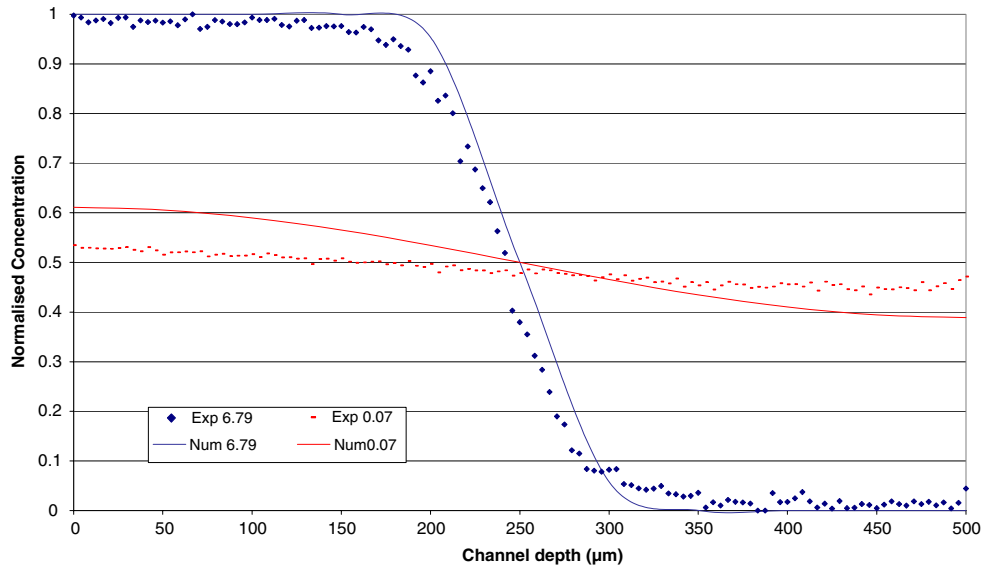

Fig. 7 Comparison between theoretical prediction of Galambos and Forster (1998) and experimental data

experimental data which is caused by a slight mismatch in flowrates delivered in the experiment. The experimental data is offset by some 10 μm indicative of a 4% difference in flowrate between the two mixing streams. This is within the bounds of the uncertainty delivered by the syringe pumps being used. Much greater deviation is observed at the lowest Reynolds number. Galambos and Forster assumed convection is the dominant mode of transport along the channel, diffusion is the dominant mode of transport across the channel, and that equal flow rates are delivered. The experimental Peclet number drops from 2,752 to 27 between the higher and lower Reynolds number. At the lowest flow rate, the offset is approximately 70 μm, which indicates greater percentage discrepancy between the flow rates in each stream. The most meaningful comparison is therefore between the slopes at the higher Reynolds number where agreement is excellent.

The phase resolution achieved in this measurement was less than that what is actually expected from the heterodyne technique. It may first seem that the velocity change, leading to pressure variation and therefore and additional term for phase difference, as the main source; but the calculated pressure difference, of $\sim$0.01 bar, would not bring any observable change. Another potential candidate is temperature fluctuations. This is not likely because of the timeframe in which data is acquired and the subtraction process implemented. Viscous heating of the fluid is not significant at the scale of the channel used for the applied flowrates. A more likely reason for the decrease in the spatial resolution is the optical transparency of the adhesive

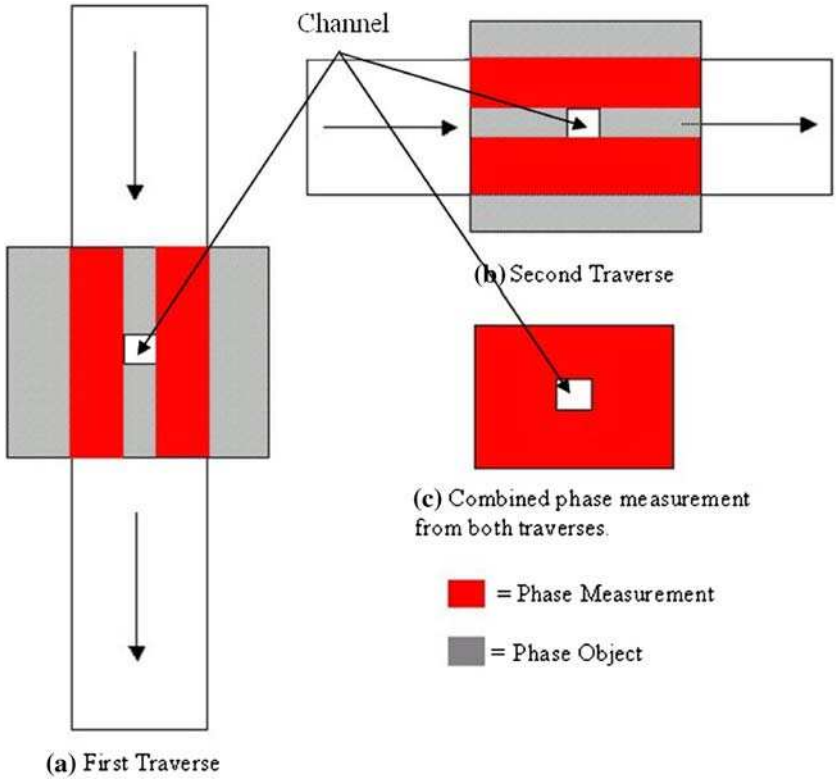

Fig. 8 Proposed solution to overcome phase accumulation due to heating of the channel material. The measurement beam traverses the test channel twice, one at right angles to the other, (**a**, **b**). Combined, the phase distribution about the channel can be determined (**c**)

film used to seal the channel. The surface of the film was coated with an adhesive layer. This layer resulted in a non-uniform refractive index across the channel. The film would also cause a refraction effect due to the surface of the film. The difficulty with such a surface is that while ideally residual phase subtraction will eliminate the effect, the complexity of the surface may render this impossible. Usually, a typical residual phase is of low frequency: a slow variation across the interferogram. However, the effect due to an adhesive layer is of much higher frequency. The subtraction process is more sensitive to higher frequency noise. For example, in the case of the micro-channel system, a change in flow rate may incur a shift in the position of the channel in the interferometric set-up. A movement of just 4 μm would result in a shift of a particular point to a different sensor pixel position for the pixel phase subtraction. This would not significantly affect a low frequency noise but the noise due to the film may result in increasing the error in the measurement rather than reducing it.

Ironically, the analysis actually demonstrated the increased accuracy of the system to distinguish errors that are often hidden in lower resolution systems. Optical quality glass would be a more suitable material to use to achieve the high resolution demonstrated previously. Alternatively, a film without adhesive placed within the optical path would result in a more uniform surface. The type of sealant used is often dictated by the system and applications, e.g. biocompatibility. Prior consideration of these effects is therefore often advantageous in material choice, resolution prediction or reduction of the effect on measurements. All the errors present are related to the interferometric set up and channel construction and are independent of the phase measurement technique. Therefore, the effects of these errors could not be eliminated by the choice of phase measurement technique. However, in the present system, despite the reduced resolution of the system the measured concentration profiles are sufficiently sampled for mass transfer measurement of a micro-fluidic system.

4.4 Application of micro-interferometry for heat transfer measurements

Using the design envelope described by Newport et al. (2004), the reduced noise in heterodyne phase retrieval open the potential for temperature profile measurement in liquids to a reasonable degree of resolution: approximately 0.1 K. However, implementation is not only hampered by the smaller phase signal but also by conduction in the device material.

In using a transparent phase object as the channel material, a difficulty arises because a temperature gradient will also be established in the channel material, which will cause a change in the thermo-optic coefficient of the device

material. Walsh and Davies (2006) discusses this for mini-systems. In order to quantify the temperature gradients in the transparent fluid, it is necessary to quantify the gradients in the channel material because the interferometer will detect the total phase change in the system. That is, the phase change in the solid plus the phase change due to the heat transfer in the fluid

$$\delta_{\text{interferometer}} = \delta_{\text{solid}} + \delta_{\text{fluid}} \tag{13}$$

Thus to measure δ_{liquid}, δ_{solid} is required. This could be achieved as follows. Two interferogrames are taken of the channel at right angles to each other, as shown in Fig. 8. Each traverse allows the phase accumulation either side of the channel in the solid to be determined. Combining two right angled traverses allows the total phase accumulation in the solid surrounding the channel to be measured. Using the channel wall as a reference would help overcome mapping pixel location errors due to the rotation.

The phase change due to temperature gradients in the channel can then be determined from

$$\delta_{\text{fluid}} = \delta_{\text{interferometer}} - \delta_{\text{solid}} \tag{14}$$

Recall from Eq. 2 that the length over which the phase change occurs is an important parameter. With thermal measurements, and concentration measurement if the channel material is porous to any appreciable extent, this length is greater than the channel dimension and is not an independent parameter. It must be determined for each experiment, but can be measured from the interferograms. An advantage of the increased length is that the sensitivity of the method is linearly increased. To date, thermal measurements have not been achieved, but micro-interferometry with heterodyne phase retrieval using CMOS cameras does offer a means of realising such measurements.

5 Conclusion

The present study compares heterodyne interferometer with phase shifting interferometer. It highlights the temporal deviation of phase difference and resolution achieved in both techniques. The following conclusions are made:

- About six times more temporal deviation in phase shift interferometry in comparison to heterodyne interferometry. Thus higher resolution and precision could be obtained using heterodyne technique and CMOS camera.
- The phase measurement limit of the phase stepping technique is over five times worse than it is for the heterodyne technique.
- The resolution achieved by the heterodyne technique is six times greater and just twice the resolution limit of λ/1,000. The resolution achieved in heterodyne interferometry clearly shows that it could be a possible candidate for measuring the microscale behaviour.
- Heterodyne interferometer could measure the variation of concentration across a 500 μm micro-channel, for different flow velocities.
- Phase accumulation and additional path length in micro-fluid device materials must be accounted for if temperature data is to be obtained.

References

Chaudhari AM, Woudenberg TM, Albin M, Goodson KE (1998) Transient liquid crystal thermometry of microfabricated PCR vessel arrays. J Microelectromech Sys 7(4):345–355

Christofferson J, Vashaee D, Shakouri A (2001) Real time sub-micron thermal imaging using thermoreflectance. In: ASME international mechanical engineering congress and exposition, New York

Creath K (1988) Phase-measurement interferometry techniques. In: Wolf E (ed) Progress in optics, vol XXVI

Creath K (1991) Phase-measurement interferometry: beware these errors. SPIE 1553:213–220

Creath K (1994) Phase-shifting holographic interferometry. In: Rastogi PK (ed) Holographic interferometry, principles and methods. Springer, Heidelberg

Dombrowski N, Foumeny EA, Ookawara S, Riza A (1993) The influence of Reynolds number on the entry length and pressure drop for laminar pipe flow. Can J Chem Eng 71:472–476

Fung TH, Chao S, Peach JE, Meldrum DR (2006) Liquid crystal thermography of an on-chip polymerase chain reaction micro-thermocycler. Paper ICNMM2006–96175, proceedings of ICNMM2006 4th international conference on nanochannels, microchannels and minichannels, Limerick, Ireland, June 19–21

Galambos P, Forster FK (1998) "Microfluidic diffusion coefficient measurement"micro total analysis systems vol 98. In: Proceedings from the μTAS '98 Workshop, Banff, Canada, 13–16 October 1998, pp 189–191

Garimella SV, Sobhan CB (2002) Transport in microchannels—a critical review.in: Annual review of heat transfer, vol XVII

Garvey J, Newport D, Dalton T (2004) Liquid diffusion measurement in micro/mini channels from full-field digital phase measurement interferometry (PMI). Second international conference on microchannels and minichannels. Rochester, NY, pp 429–437

Hapke I, Boye H, Schmidt J (2002) Flow boiling of water and n-heptane in microchannels. Microscale Thermophys Eng 6(2):99–115

Hariharan P, Oreb BF, Eiju T (1987) Digital phase-shifting interferometry: a simple error-compensating phase calculation algorithm. Appl Opt 26(13):2504–2507

Hetsroni G, Mosyak A, Segal Z, Pogrebnyak E (2003) Two-phase flow patterns in parallel micro-channels. Int J Multiphase Flow 29:341–360

Hohreiter V, Wereley ST, Olsen MG, Chung JN (2002) Crosscorrelation analysis for temperature measurement. Meas Sci Technol 13:1072–1078

Kafri O (1989) Fundamental limit on accuracy in interferometry. Opt Lett 14(13):657–658

Malacara D, Rizo I, Morales A (1969) Interferometry and the Dopplereffect. Appl Opt 8(8):1746–1747

Malacara D, Servin M, Malacara Z (1998) Interferogram analysis for optical testing. Marcel Dekker, New York

Massie NA, Nelson RD, Holly S (1979) High-performance real-time heterodyne interferometry. Appl Opt 18(11):1797–1803

Mayinger F (1993) Image-forming optical techniques in heat transfer: revival by computer aided data processing. J Heat Transf 115:824–834

Merzkirch M (1987) Flow visualisation. Academic, New York

Newport D, Garvey J, Whelan M, Dalton T, Egan V (2004) Development of optical temperature measurement procedures for the micro-scale. J Microscale Thermophys Eng 8 (2) :141–154

Patil VA, Narayanan V (2005) Application of heated-thin-foil thermography technique to external convective microscale flows. Meas Sci Technol 16:472–476

Sato Y, Irisawa G, Ishizuka M, Hishida K, Maeda M (2003) Visualization of convective mixing in microchannels by fluorescence imaging. Meas Sci Technol 14:114–121

Walsh PA, Davies MRD (2006) Factors affecting temperature measurement using phase measurement interferometry in small scale devices. Exp Therm Fluid Sci 30(8):853–862

Wereley ST, Gui L, Meinhart CD (2002) Advanced algorithms for microscale particle image velocimetry. AIAA 40(6):1047–1055